Journal of Alloys and Compounds 509 (2011) 9528–9535

Contents lists available at ScienceDirect

Journal of Alloys and Compounds

journal homepage: www.elsevier.com/locate/jallcom

An XANES and XES investigation of the electronic structure of indium rich $In_xGa_{1-x}N$ films

I.N. Demchenko[a,b,c,*], M. Chernyshova[d], E. Piskorska-Hommel[c,e], R. Minikayev[c], J.Z. Domagala[c], T. Yamaguchi[f], W.C. Stolte[a,b], K. Lawniczak-Jablonska[c]

[a] University of Nevada Las Vegas, Department of Chemistry, 4505 Maryland Pkwy-Box 454003, Las Vegas, NV 89154-4003, USA
[b] Lawrence Berkeley National Laboratory, ALS, 1 Cyclotron Rd., Bldg 7R0201, Berkeley, CA 94720-8225, USA
[c] Institute of Physics PAS, al. Lotnikow 32/46, 02-668 Warsaw, Poland
[d] Institute of Plasma Physics and Laser Microfusion, 23 Hery Street, 01-497 Warsaw, Poland
[e] Institute of Solid State Physics, University of Bremen, Bulding NW1, Otto-Hahn-Allee, 28359 Bremen, Germany
[f] Res. Org. of Sci. & Eng., Ritsumeikan Univ., Shiga, Japan

ARTICLE INFO

Article history:
Received 5 April 2011
Received in revised form 19 July 2011
Accepted 20 July 2011
Available online 27 July 2011

PACS:
78.70Dm
78.70En
61.05.cj
61.05.cp

Keywords:
XANES
FEFF
XES

ABSTRACT

The electronic structure of InGaN epitaxial layers grown on sapphire substrates was studied using X-ray absorption at the In L_3 and N K edges, as well as N K_α X-ray emission. Knowing that the InGaN crystallizes in an anisotropic wurtzite structure, the linear polarization of synchrotron radiation was exploited to estimate the influence of the crystal structure anisotropy on the distribution of the local density of states at the site of In and N. The calculated partial density of states describes the observed anisotropy in the measured spectra. Influence of the core–hole effect on the analyzed absorption spectra was verified and reveal that a core hole potential is effectively screened by the surface mobile electrons for the sample with maximum indium content. The bandgap values were provided for the investigated InGaN alloys and were found to vary preudo-lineary with indium content.

1. Introduction

Despite widespread application in optoelectronic and electronic devices, such as in white light emitting diodes and blue laser diodes, there are still many open questions concerning the basic material properties of group-III nitrides. The ternary (In,Ga)N compound covers the spectral range from the infrared (InN with a bandgap around 0.7 eV [1]) up to the near UV (GaN with 3.42 eV [1]). Unfortunately, this compound is not stable over the whole composition range. Bimodal and spinodal decomposition occurs and the ternary compounds remain stable only for In-contents less than 20% or greater than 80% [2]. This instability range has been also shown to depend upon the strain state of the epitaxial layers [3]. In order to gain more knowledge about this range, the study of $In_xGa_{1-x}N$ layers with a high In content were performed. The X-ray absorption near edge structure (XANES) and X-ray emission spectroscopy (XES) techniques were used to help understand its local atomic order and electronic structure.

XANES focuses on the region of the X-ray absorption spectrum dominated by multiple photoelectron scattering and is a powerful tool to analyze the electronic structure of materials. The spectral fine structure is very sensitive to changes in the chemical environment around a selected element [4] and provides information about the ionic state of the absorbing atom, electron configuration, and site symmetry. Moreover, a simultaneous modification of the conduction band (CB) and valence band (VB) by In incorporation into GaN can be studied with X-ray absorption spectroscopy (XAS), which yields the energy difference between the core level and the unoccupied CB, and XES, which yields the energy difference between the occupied VB and the core level. Together, XAS and XES measurements can be used to evaluate the size of the bandgap [5] in way that optical absorption cannot, namely, tracking the dynamics of the CB in conjunction with VB modifications close to the Fermi level.

The InGaN system crystallizes in a wurtzite structure with two kinds of first-neighbor anion–cation bonds [8]: a single bond along the c-axis (π bond) and three bonds slightly inclined with respect

* Corresponding author. Fax: +1 510 486 7588.
E-mail address: INDemchenko@lbl.gov (I.N. Demchenko).

0925-8388/$ – see front matter © 2011 Elsevier B.V. All rights reserved.
doi:10.1016/j.jallcom.2011.07.059

to the *c*-plane (σ bonds), see insert in Fig. 3. For InN, the three σ bonds length is about 2.16 Å, being slightly longer than the π bond which is about 2.15 Å. On the other hand, for GaN it is the opposite, with the σ bond of about 1.95 Å being slightly shorter than the π bond of about 1.97 Å [6,7]. This anisotropy may influence the optical as well as the transport properties and, therefore, highlights the importance of experimental observation of bond strength distributions along different crystal orientations: along the *c*-axis or in *c*-plane. Therefore, in this paper the spatial electronic orbital distribution around an absorbing atom are examined by varying the direction of the linearly polarized synchrotron radiation (SR) with respect to the specific crystallographic direction in wurtzite InGaN films [8,9].

Additionally, the simulations of the XANES spectra by *ab initio* calculations under the assumption of the supposed local atomic arrangement compared to experimental spectra are presented. The models were refined iteratively to obtain the best agreement with experimental results. This approach was used here to get information about the local atomic order and electronic structure in the materials studied. The linear polarization of synchrotron radiation and core–hole effect were considered in calculations.

2. Experimental

The $In_xGa_{1-x}N$ ($x = 0.23$, 0.35 and 0.53) samples were grown 0.4 μm thick on the nitridated *c*-plane of the sapphire substrates without a GaN buffer at a temperature of 550 °C using radio-frequency plasma-assisted molecular beam epitaxy (RF-MBE). InN and GaN reference samples of approximately 1.0 μm were prepared using the same procedure [10].

XANES spectra were collected at room temperature, at the Advanced Light Source (ALS) on beam lines 9.3.1 and 8.0.1, with respective energy resolutions of 0.6 eV near the indium L_3 edge, and 0.2 eV near the nitrogen *K* edge. In order to avoid self absorption effect due to the high content of indium, XANES spectra were gathered in a total electron yield (TEY) detection mode, by measuring the sample drain current. Soft X-ray emission (XES, 8.0.1) was measured using the Tennessee/Tulane grating spectrometer [11] which has a total energy resolution of approximately 0.6 eV. The elastic emission peak in XES spectra was used for calibration of the detector energy to the XAS monochromator energy. All of the presented XANES spectra were averaged through at least two data sets, next a pre-edge linear background was subtracted and the edge step was normalized to unity.

XANES spectra were acquired with two different angles between the sample surface (*c*-plane) and the polarization vector of SR, *e*. In case of the "*in-plane*" geometry the polarization vector *e* was parallel to the sample surface, thus, the electronic transitions are excited mainly in the "*c*-plane" probing the σ bonds. In the "*out-of-plane*" geometry the polarization vector *e* formed a small angle with the "*c*-axis", which is normal to the sample surface. Therefore the states localized along the "*c*-axis", single π bond, predominate in the spectra. Additionally, data at the nitrogen *K* edge were collected at 45° angle between the polarization vector of SR and the sample surface to obtain an 'average' XANES spectra, which were used to estimate the size of energy gap.

To examine possible phase segregation and the level of structural disorder in the investigated structures the high resolution X-ray diffraction (HRXRD) measurements were carried out using a high-resolution diffractometer (Philips X'Pert-MRD) equipped with a parabolic X-ray mirror, a four-bounce Ge 220 monochromator at the incident beam, and a three-bounce Ge analyzer at the diffracted beam.

3. Calculations

The calculation of the XANES spectra, were performed using *ab-initio* multiple-scattering FEFF8 [15] and FDMNES [16] codes. The FEFF8 code implements a one-electron theory based on a self-consistent (SC) real-space Green's-function formalism and final-state potentials taking into account an appropriately screened core–hole (CH). FDMNES code provides two different approaches for monoelectronic calculations: (i) a finite difference method to solve the Schrödinger equation, where the shape of the potential is free, thus a Muffin-Tin (MT) approximation can be avoided; or (ii) Green formalism (multiple scattering) with a MT potential. We applied the second approach, not only to ensure the similarity between FEFF8 and FDMNES codes, but to show the projected densities of states along different crystallographic directions ($p_{x,y,z}$ and so on). Such an option is inaccessible in FEFF8.

The following values of the lattice constants used in calculations were taken from the our XRD measurements: InN – $a = b = 3.5331$ Å, $c = 5.7063$ Å; GaN – $a = b = 3.18940$ Å, $c = 5.18614$ Å; and $In_{0.23}Ga_{0.77}N$; $a = b = 3.250$ Å, $c = 5.3039$ Å. The space group is $P6_3mc$. The positions/coordinates of the atoms in each cluster, except for the $In_{0.23}Ga_{0.77}N$ alloy, were taken from crystal structures of *w*-InN and *w*-GaN compounds [6,7]. In the case of the $In_{0.23}Ga_{0.77}N$ alloy calculations were done for different models based on an ideal *w*-GaN structure (two atoms of Ga and two atoms of N per unit cell) where 0.5 atom of Ga was replaced by indium. The best results were obtained for indium atoms located at the down corner positions of the unit cell and around the central (absorber) indium atom. The following coordination shells were considered, counting from the absorber: (1) 3 × N – 1.99 Å and 1 × N – 2.0 Å; (2) 6 × Ga – 3.25 Å and 6 × In – 3.25 Å; (3) 1 × N – 3.30 Å, 3 × N – 3.81 Å and 6 × N – 3.82 Å; (4) 6 × Ga – 4.6 Å; (5) 6 × N – 4.63 Å, 6 × N – 5.01 Å and 3 × N – 5.02 Å; (6) 2 × Ga – 5.30 Å and 12 × Ga – 5.63 Å, and so on.

The following assumptions in the FEFF8 input file were used to simulate measured XANES spectra and to get partial densities of states (PDOS): final states were calculated inside a sphere of about 13 Å radius; the muffin tin (MT) radius was calculated using the Norman procedure and MT spheres were automatically overlapped by 10%; only the dipole component was taken into account; the real Hedin and Lundqvist exchange-correlation potential was used; all near-edge structure was specified up to $k = 4$ Å^{-1}, and all of the states below the Fermi level were considered to be occupied. To eliminate the contribution of the occupied states into the absorption spectra the transition cross section for these states was set to zero and the convolution with the Lorentzian function was performed. Using the above assumptions, the position of the Fermi level for the L_3 edge of indium was found to be at −7.72 eV for InN and at −8.01 eV for $In_{0.23}Ga_{0.77}N$ alloy. The Fermi energy was then shifted down in energy by 0.7 eV for both models in order to set the Fermi level in the middle of the bandgap.

The FDMNES simulations were done using input parameters similar to those used in the described FEFF8 calculations, with the exception that the E_F value was shifted by −4.7 eV.

4. Results and discussion

4.1. DOS resulted from FEFF code

In order to find the origin of the main features in the experimental XANES spectra the total and PDOS were selectively compared to them. In Figs. 1 and 2 the calculated, using the FEFF8 code, total and partial ground-state DOS for occupied and unoccupied states for *w*–InN, *w*–GaN and $In_{0.23}Ga_{0.77}N$ alloy are presented. It should be emphasized that, originally, zero on energy scale in the DOS calculated by FEFF8 corresponds to the vacuum level, which is typically several eV above the self consistently determined Fermi level. The data in these two figures are shown on a relative energy scale, E-E_F, where E_F was calculated using FEFF8.

Comparing the total DOS with the PDOS one can anticipate which states significantly contribute to the given structure seen in the electronic state distribution. Consequently, the peak marked as "*A*" in Fig. 1(a) corresponds to the VB maximum, and according to PDOS calculations is composed mainly of N 2*p* states together with a smaller amount of indium *p* and *d* states. Peak "*B*" is in the CB and is defined by intermixing of all of the indium and nitrogen states with approximately equal proportion. A double structure "*C*", located about 5 eV, is mainly composed of *p*-N and *s*-In states with a small contribution of indium *p* and *d* states. A peculiarity labeled as "*D*" at about 8.9 eV is formed by the mixture of *p* orbitals primarily from In with a small contribution from N. The "*E*" and "*F*"

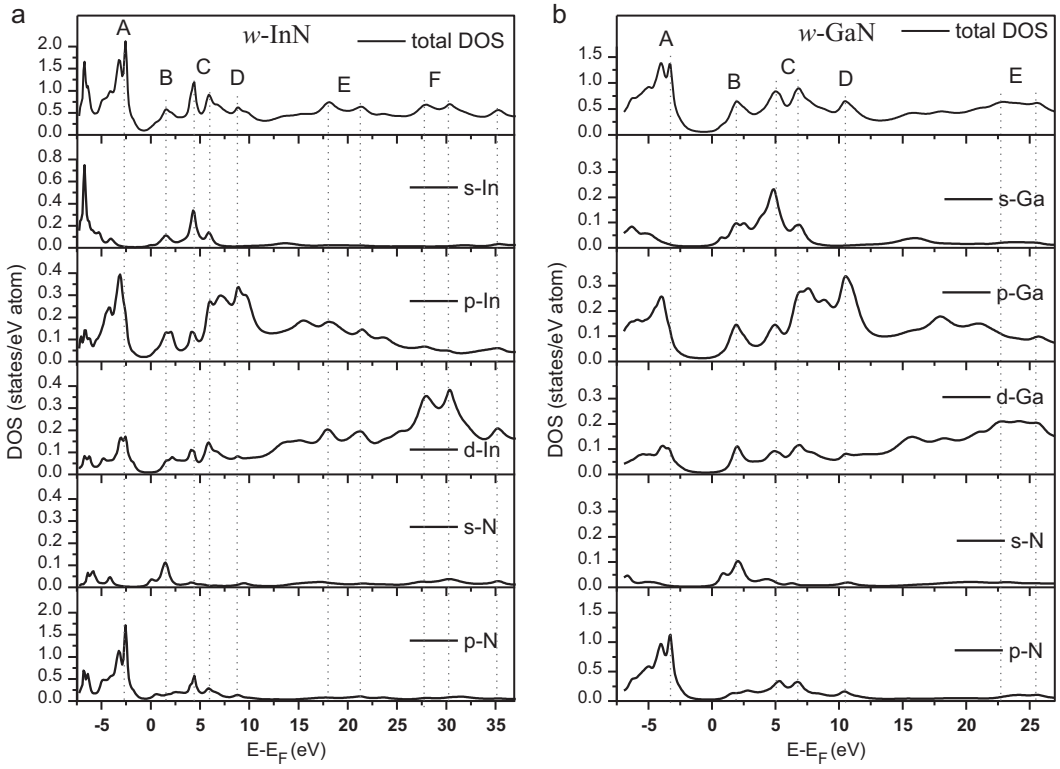

Fig. 1. Total and partial *s*, *p*, *d*-In; *s*, *p*-N densities of states for (a) *w*-InN and (b) *w*-GaN calculated using FEFF8 code.

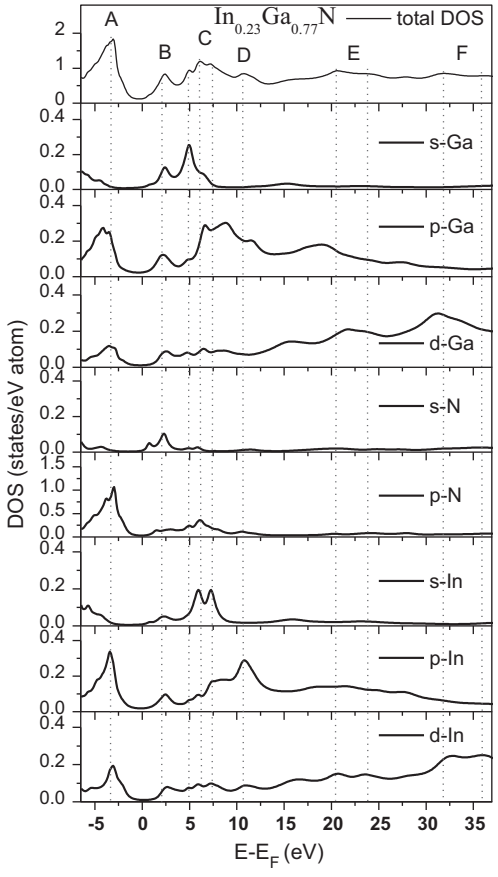

Fig. 2. Total and partial *s*, *p*, *d*-Ga; *s*, *p*, *d*-In; *s*, *p*-N densities of states for $In_{0.23}Ga_{0.77}N$ alloy calculated using FEFF8 code.

double structures are stipulated by *d* and *p* states of In and a smaller statistical weight of N *p* states.

For *w*–GaN the specific contributions of PDOS of individual elements to the main features of GaN total DOS are followed the ones for the InN (see Fig. 1(b)). In turn, adding indium atoms into GaN significantly changed the electronic structure, as can be seen by comparing the total and partial DOS in Figs. 1 and 2. For $In_{0.23}Ga_{0.77}N$ alloy the most profound change is a smearing of the well separated, in the binary compounds, "*C*" structure, due to the overlap of In and Ga *s* states, and *p* states from Ga, In and N. In the following, we use these peculiarities of the electronic states energy distribution to interpret the origin of XANES spectral features taking into account the transition probability for a given symmetry of electronic states and a given geometry of spectra registration.

4.2. Polarized XANES: indium L_3 – and nitrogen K edges

Under the assumption of dipole selection rule the L_3 edge involves the electronic transitions from the atomic-like indium $2p_{3/2}$ state to unoccupied states above the Fermi level with *s* and *d* symmetry. In Fig. 3 we present experimental XANES spectra gathered at two different geometries near the indium L_3 edge for the $In_xGa_{1-x}N$ layers with indium content of 1, 0.53, 0.35 and 0.23. The nitrogen *K* edge under the same assumption involves transitions from an atomic-like N 1*s* state to the unoccupied states of *p*-character above the Fermi level. The experimental spectra for the same samples and for two geometries are presented in Fig. 4.

As can be seen by comparing Figs. 3 and 4, the anisotropy for the *p* conduction states distribution at the anion site is more pronounced as related to the *d* states at the cation site. It is attributed to the different atomic orbitals responsible for the *K* and L_3 edges. As was explained above, due to the dipole selection rule, the *K* edge spectra in anisotropic wurtzite structures are composed of

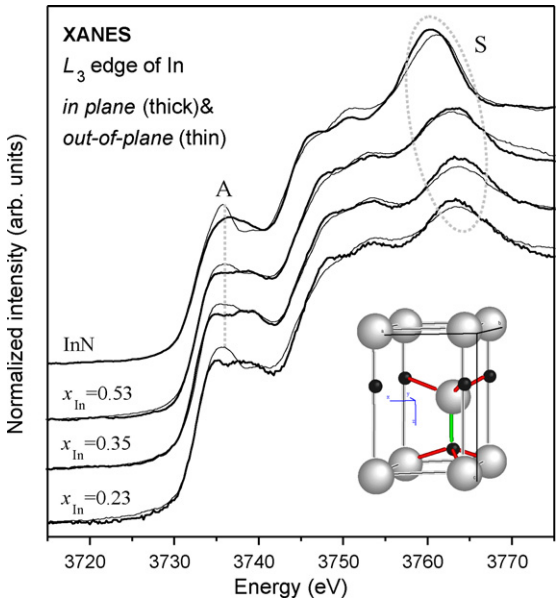

Fig. 3. Experimental XANES spectra at the L_3 edge of indium for the examined samples (from top to down): InN, $In_{0.53}Ga_{0.47}N$, $In_{0.35}Ga_{0.75}N$ and $In_{0.23}Ga_{0.77}N$ layers; the spectra were collected for two geometries (thick line–"*in-plane*" and thin line–"*out-of-plane*" geometry). The insert presents the unit cell corresponding to *w*-InN. Grey balls denote In atoms, black ones–N.

a mixture of $p_{x,y}$ and p_z components with a varying ratio determined by the experimental conditions. Therefore, the *K* edge of N reflects asymmetric *p*-type orbitals, while the indium L_3 edge reflects orbitals with *s* and mainly *d* symmetry. The *s* orbitals are spherical and *d* orbitals, because of their spatial orientation, contribute partially in both geometries of the experiment, giving a less asymmetric XANES spectra at this edge. Moreover, the observed less-pronounced anisotropy at the cation site could be additionally attributed to significantly better energy resolution at the nitrogen *K* edge considering its much smaller natural core–hole level width (0.11 eV [12]) as compared to the indium L_3 edge (2.65 eV [13]).

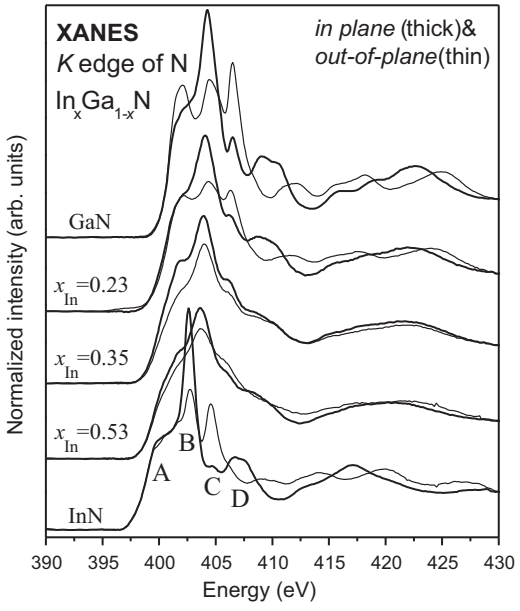

Fig. 4. Nitrogen *K* edge XANES spectra for investigated samples with different In content collected for different geometries: "*in-plane*" (thick line)) and "*out-of-plane*" (thin line).

We start from the qualitative comparison of the indium L_3 edge spectra. There is no observable energy shift in the position of the absorption edge for the investigated samples regardless of the applied geometry of measurement. Therefore, within the limit of the experimental energy resolution, the compositional changes have no influence on the ionic state of the indium, keeping unchanged the charge transfer in the In-N bounding irrespective of the geometry of bond. The observed fine structure, between 3730 and 3743 eV, is more extended for alloys in comparison to the InN film. A shoulder, arising in the region of 3741–3747 eV, gradually moves to higher energy reaching a maximum of 0.6 eV relative to the pure InN. The resonance, marked as "*S*", at about 3760–3765 eV, also shifts by 2.2 eV towards higher energies as the indium content is decreased. These changes in the absorption spectra are evidence for the following: increasing the content of Ga atoms into InGaN induces an additional asymmetry in the crystal field of the InN host matrix due to the relatively shorter bonds of gallium atoms with nitrogen. The Ga-introduced crystal field changes enhance the energies of some higher-energy indium *d* orbitals decreasing the intensity of the feature "*S*" with increasing Ga content, Fig. 3. The effect is also clearly visible on the PDOS presented in Figs. 1a and 2 thus properly accounted in simulation.

For the "*out-of-plane*" geometry the peak labeled "*A*" (see Fig. 3) has a larger amplitude for the InN and $In_{0.23}Ga_{0.77}N$ than for the other two alloys. This feature also exists for the remaining two alloys, but with less intensity and less localization as compared to the InN. This demonstrates the higher local structural disorder in layers containing more than 0.23 of indium. In addition, the "*S*" peak corresponding to "*out-of-plane*" geometry, for both the InN and $In_{0.23}Ga_{0.77}N$, is slightly shifted to higher energies compared to their respective "*in-plane*" spectrum. This polarization dependent effect can be explained by varying contribution of unoccupied d_{z^2}, $d_{x^2-y^2}$ and d_{xy} electron orbitals. The ratio of these orbitals depends upon the orientation of the SR electric field along the specific crystallographic directions of the investigated film (will be shown below, see Section 4.2.1). The alloys with $x_{In} = 0.35$ and 0.53 do not show this effect. The loss of the anisotropy is even more pronounced at *K* edge of N for the samples with high content of In. This suggests that the InGaN alloys, containing more than 0.23 of indium, may be grown with some structural misorientation, i.e., crystallites in these films are not well aligned with respect to the growth direction averaging, thus, the anisotropy of crystal. Moreover, we cannot exclude the possibility of phase segregation.

Subsequently, to confirm this, all of the samples were examined by HRXRD. Our HRXRD measurements proved that a mosaic structure indeed exists with a tilt mosaicity deflected from the direction of growth by about 1° in the layers with $x_{In} = 0.35$ and 0.53, as opposed to the sample with $x_{In} = 0.23$ which exhibited a quite good crystalline arrangement. Moreover, it was observed, similarly to the work in ref [14], that the $In_xGa_{1-x}N$ alloys with 0.35 and 0.53 indium content are not chemically homogeneous. One final HRXRD observation was the detection of a small amount of pure indium phase in the sample with $x_{In} = 0.53$. These results support our XANES observations and conclusions. Therefore, more quantitative interpretations of the XANES spectra based on theoretical simulations were only performed for the pure InN and GaN samples, and the $In_{0.23}Ga_{0.77}N$ alloy.

In Fig. 5 comparison of the calculated XANES spectra and PDOS for InN and $In_{0.23}Ga_{0.77}N$ alloy with the experimental results is presented. For both samples the main features in the L_3 spectra closely follow a mixture of the In *d*-PDOS with insignificant amount of In *s*-PDOS. By taking into account either transitions to $l-1(s)$ or to $l+1(d)$ states symmetry in the FEFF8 code for calculations of the "unpolarized" XANES In L_3 edge spectra, one can discriminate the contribution to different symmetry states. The estimated contribution of metal *s* states into the InN spectrum is about 30 times weaker

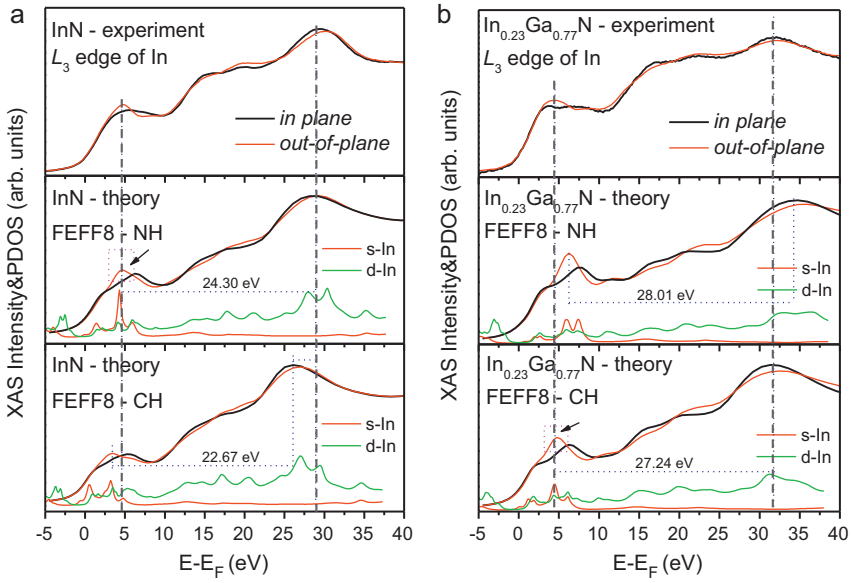

Fig. 5. A comparison between experimental and simulated XANES "*in–plane*" and "*out-of–plane*" spectra along with partial densities of states calculated by FEFF8 code (see text for details) for: (a) InN and (b) $In_{0.23}Ga_{0.77}N$ film. The simulation of XANES spectra for the indium L_3 edge was performed with (CH) and without (NH) taking into account a core–hole.

than that of *d* states. It agrees with the results obtained in [17] for the L_3 edge of Re, where the calculated ratio of the absorption cross-sections corresponding to the transitions into *d* and *s* final states is about 50:1. However, we should emphasize that close to the CBM metal, *s* orbitals are involved into hybridization with N 2*p* states and could not be neglected since they influence on modification of the low energy region of In L_3 spectrum. It was also demonstrated by *ab initio* study (WIEN2k code) of electronic and optical properties of InN in wurtzite and cubic phases [18].

Since the final state in the soft X-ray emission process contains a hole in the VB rather than the core level, the emission spectra reflect the ground-state PDOS provided that final state rule is valid. In case of X-ray absorption process, in the absence of a core hole (the initial state rule), both the initial and the final states in FEFF8 are represented by the ground-state single electron wave functions. In the presence of a core hole (the final state rule), the final state wave function is calculated for a system with a static core hole in a given core level. By default, FEFF8 calculates a XANES spectrum using an appropriately screened CH. However, the experimental spectra are not always satisfactorily reproduced because the electronic wave functions for the occupied and unoccupied bands can be significantly distorted by the presence of a CH [19]. For instance, in the soft X-ray region, there are cases where the mobile electrons of the metal completely "screen" the core–hole potential. For this situation, the NOHOLE card should be used in FEFF8. This roughly simulates the effect of complete CH screening by causing FEFF8 to calculate potentials and phase shifts as if there were no CH. To estimate the influence of the CH on the XANES spectral profile, additional calculations assuming a completely screened core hole (NH) were performed. The results are shown in the middle frames in Fig. 5. It was found that, by taking the CH into account, the experimental spectrum for the $In_{0.23}Ga_{0.77}N$ is more closely reproduced (Fig. 5(b)), whereas for the InN the NH approach should be applied (Fig. 5(a)). The experimental spectrum for the InN is blue-shifted as compared to the CH calculated spectrum, and for the region around 29.3 eV, it more closely resembles the simulated spectrum without taking into account CH (NH in Fig. 5(a), middle). The distance between the resonances, marked by vertical dotted lines in Fig. 5(a), for NH model is 1.6 eV larger compared to CH model and agrees well with the experimental one. Therefore, for the InN a CH potential seems to be effectively screened by mobile electrons. Such an effect was not observed for the $In_{0.23}Ga_{0.77}N$ alloy (see Fig. 5(b)) where the accounting for CH provides better agreement with the experiment in the considered region. Let us remember that XANES spectra were collected by means of a surface sensitive detection mode (TEY). Thus, considering the results in [21], where the existence of an electron accumulation layer at the InN surface was quantitatively confirmed, we hypothesize that the screening of the core–hole potential for InN is more effective due to the extra free surface electrons, which does not appear to be the case for the $In_{0.23}Ga_{0.77}N$ film. Additionally, in [22] a notable difference between the X-ray absorption edge onsets for the total fluorescence yield (TFY, which is bulk sensitive) and the TEY modes was observed for nitrogen *K* edge of InN. The onsets were found to occur at approximately 0.8 eV and 1.4 eV above the valence band maximum, respectively. The authors attributed the shift of the absorption threshold for the TEY XAS by pinning of the Fermi level at the surface high above the conductive band minimum, due to the intrinsic electron accumulation. These results confirm our assumption about screening of CH potential for indium L_3 edge of InN.

Many authors have previously performed simulations of XANES spectra for InGaN alloys near the *K* edge of nitrogen, see for instance [19,20], therefore we have chosen not to discuss nitrogen spectra by comparing with FEFF calculations. Instead we will examine the general trends observed in spectra. When a chemical bond interacts with incoming radiation at a large incidence angle ("*in-plane*" geometry), the σ-bonds play a significant role, resulting in strong absorption being observed for the transition from N 1*s* to the unoccupied $p_{x,y}$ states. Similarly, for a grazing incidence angle ("*out-of-plane*" geometry), the strong absorption is dominated by the transition from N 1*s* to the unoccupied p_z state which corresponds to a π-bond character. In Fig. 4, the peak labeled "C" in the "*out-of-plane*" geometry corresponds to p_z final states, while the peaks labeled "A", "B", and "D" – correspond to $p_{x,y}$ final states.

The XANES spectra of nitrogen *K* edge, indium L_3 edge and HRXRD confirm high structural disorder in the $In_{0.35}Ga_{0.65}N$ and $In_{0.53}Ga_{0.47}N$ alloys. For both alloys the measured XANES spectral features show peak broadening and no polarization dependence.

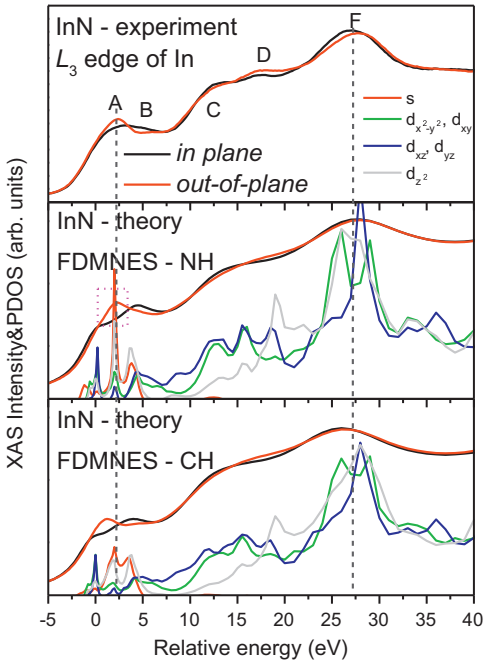

Fig. 6. Experimental (top) and calculated XANES L_3 indium spectra for the InN layer (for different geometries) applying FDMNES code: middle – with (CH) and, bottom – without (NH) core–hole; projected DOS for In atom are also shown.

This serves as a fingerprint of non-ideal hexagonal structure. Such behavior suggests an increasing randomness in the nitrogen atomic arrangement, primarily caused by misorientation of the crystallites. The $In_{0.23}Ga_{0.77}N$ layer exhibits a behavior similar to that of the GaN polarized spectra.

4.2.1. DOS resulted from FDMNES code

To gain additional information about projected PDOS contribution for In L_3 edge we performed calculations using the FDMNES code for both the total atomic electron density and the projected density of states for each l and m, where l is the orbital angular momentum number and m is the magnetic quantum number. As can be seen in Fig. 6, and similar to our FEFF8 results in Fig. 5(a), the NH approach more closely reproduces the experimental XANES spectrum of InN. Together with the simulated XANES spectra we show the PDOS for the In s and $d_{x^2-y^2}$, d_{xy}, d_{yz}, d_{zx}, d_z^2 projected orbitals. Partially, they contribute in both geometries of experiment, but some asymmetry of states can be noticed and is reflected in the features of XANES spectrum. The primary features in these spectra reflect mainly In d_z^2 and $d_{x^2-y^2}$, d_{xy} PDOS for "*out-of-plane*" and "*in-plane*" geometries, respectively. For the "*out-of-plane*" geometry, peak "*A*" is shown to be composed mainly of d_z^2 states. It decreases in intensity on the theoretical XANES spectrum in case of "*in-plane*" geometry, where some discrepancy between the theoretical and experimental spectra exists due to, probably, underestimation of the lowest $d_{x^2-y^2}$, d_{xy}, $d_{xz,\,yz}$ states contribution in this region. Inexpressive regard to the theory, feature "*B*" ("*in-plane*" geometry) is associated with the $d_{x^2-y^2}$, d_{xy}, $d_{xz,\,yz}$ contribution. The larger amplitude of the "*D*" feature ("*out-of-plane*" geometry) could be explained by occurrence there of significant contribution of In d_z^2 orbitals. A higher energy shift of the "*F*" resonance ("*in-plane*" versus "*out-of-plane*" geometry) can be attributed to differing contributions of $d_{x^2-y^2}$, d_{xy} orbitals and $d_{xz,\,yz}$ for the different orientations.

The performed calculations confirm the observed changes in the intensity of XANES spectra measured in different geometries, and describe them by PDOS anisotropy. The geometrical effect is weaker in case of the XANES L_3 edge of indium compared to the nitrogen K edge. In spite of that the influence of CH effect on XANES spectra for indium L_3 edge for InGaN alloys is evident.

4.3. "Unpolarized" XAS and XES near the K edge of nitrogen

In Fig. 7 the results for the $In_xGa_{1-x}N$ samples measured by XES (K_α line) and XANES for the nitrogen K edge are presented. All of the data were collected at the angle of 45° between the incidence beam and the sample surface.

Fig. 7(a) presents a series of soft X-ray emission spectra collected at an incident photon energy above the absorption threshold, nominally 403.4 eV. By recording N K_α emission spectra we study the occupied 2p states of N. A narrowing of $In_xGa_{1-x}N$ VB with increasing indium content is clearly visible and agrees with the energy distribution of 2p-N states for InN and GaN presented in Fig. 3, where was shown that the N states are more localized in InN than in GaN. Two distinct features appear in the discussed region. The binding energy at the top of the VB is shifted up in energy by approximately 0.2 eV as the In content is decreased, whereas the bottom of the VB is moved up by about 1.2 eV. A maximum observed around 394 eV, at the top of the VB, is assigned to 2p-N occupied states. The low-energy feature located between 388 and 391.5 eV is primarily composed of nitrogen 2p states hybridized with indium 5s and gallium 4s states. Likewise, with increasing indium content in GaN, the CB minimum moves towards lower energy, which can be explained by an increasing amount of near neighbor In atoms. This reflects the change in the bandgap of the nitrogen projected states due to the some fraction of N atoms is bound to Ga and part to In which have different gaps.

A comparison of XES/XANES spectra in Fig. 7(a and c) shows a modification of the bandgap size taking place primarily by the reorganization to higher energies of the bottom of the CB with decreasing indium content.

Additional measurements were performed for the InN and for the $In_xGa_{1-x}N$ alloys at excitation energies of 397.15 and 397.9 eV, close to their CB minima (absorption onsets), to determine if the bandgaps are of direct or indirect type [23]. In a XES experiment the bandgap type can be determined by observing the emission spectra as a function of excitation energy. For a direct energy gap material, emission at the highest energy is expected for excitation energy in the vicinity of the absorption threshold (into the CB minimum, CBM). As the excitation energy increases, the emission should shift towards lower energy. For indirect bandgap materials an opposite behavior is expected, i.e., a shift of the emission spectrum (namely top of the VB, VBM) towards higher energy as the excitation energy increases. In another words, as the excitation energy increases, the probing transitions get closer, in k space, to the top of the VB [5]. As seen in Fig. 7(b), emission data for InN clearly show the tendency expected for a direct energy gap. Namely, the XES spectra for the InN film recorded at two different excitation energies, just below the absorption threshold 397.15 eV and slightly above the first resonance 403.4 eV, show a shift of the VBM to lower energies indicating a direct bandgap. This behavior results from a well-established k-selectivity effect [24], whereby restrictions on the intermediate state relaxation relatively enhance the emission at the k-point of the CBM.

Emission spectra with an excitation energy close to the CBM were compared to their respective XANES spectra for all of the investigated samples, direct energy gap values were then estimated by observing the difference between the top and the bottom of VB and CB.

The resulting direct energy gap values are plotted versus indium content (x_{In}) in Fig. 7(d). They are consistent with those of Davydov

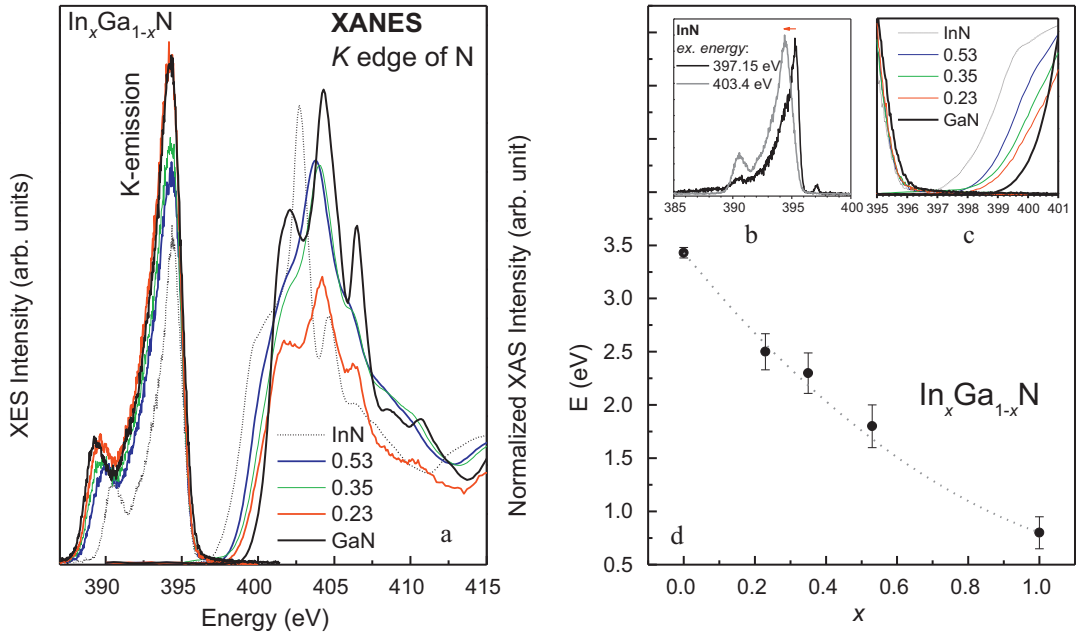

Fig. 7. (a) Nitrogen *K* edge X-ray emission spectra (left side: short dots line–the InN; blue line – $x = 0.53$; green line – $x = 0.35$; red line – $x = 0.23$; thick black line – the GaN) and absorption spectra (right side: the same notation as for emission lines) of the $Ga_{1-x}In_xN$ layers with different compositions of indium. (b) Nitrogen emission spectra of InN for two excitation energies. (c) Zoomed region of nitrogen *K* edge XAS and XES spectra for different In content. (d) The dashed curve corresponds to the fit of the band gap energies using bowing parameters equal to 1.43 eV. The points on the plot correspond to the energy gap values estimated from collation of XES and XAS experimental data for investigated samples. (For interpretation of the references to color in this figure legend, the reader is referred to the web version of the article.)

et al. [1]. Theoretically, the behavior of the gap for such an alloy system can be described by the following formula [25]:

$$E_G(x) = 3.42x + 0.77(1 - x) - bx(1 - x),$$

where x is the Ga composition. Early optical studies gave a wide range for the bowing parameter, b, ranging between +4.9 eV and −0.8 eV [26], however, recent comprehensive optical absorption studies of high-quality $In_xGa_{1-x}N$ films have found that $b = 1.43$ eV [25]. Our data indicate that the energy gap values vary pseudo-linearly with x. The dashed line in Fig. 7(d) corresponds to the predicted position if the bowing parameter b equals to 1.43, which agrees well with the previous optical absorption studies [25].

5. Conclusions

XES/RIXS and angle-dependent XAS studies of *w*-InN, *w*-GaN and $In_xGa_{1-x}N$ (with $x = 0.23, 0.35, 0.53$) layers were performed. We have provided reliable spectra of indium L_3 and nitrogen *K* edges with theoretical calculations of the selective spectra including the CH effect and PDOS projected on different crystallographic directions. By applying FEFF8 and FDMNES codes we have shown that the CH should be included for the calculation of unoccupied states in the case of the InGaN alloys. For pure InN the NH approach better describes the experimental data, which we believe is due to an accumulative layer effect causing a higher concentration of free carriers in InN that fully screen the core level with a hole. Our calculations for these samples are in good agreement with the reported XANES measurements for two geometries "*in-plane*" and "*out-of-plane*", and prove that calculations using the FDMNES code for In *s* and *d*-PDOS can fully describe the fine structure observed in the spectra. In the case of the $In_xGa_{1-x}N$ layers the geometrical effect can be a test for the quality of grown layer.

Combining XES/RIXS and XANES at the *K* edge of N for the samples with a varying content of In, we have proved that their bandgap reorganizes mainly by moving the bottom of CB preudo-lineary upward in energy with decreasing of In content.

Acknowledgements

The authors wish to thank the staff of the ALS for their excellent support (especially P. Olalde-Velasco and W. Yang). This work was performed at the ALS which is supported by the Director, Office of Science, Office of Basic Energy Sciences, of the U.S. Department of Energy under Contract No. DE-AC02-05CH11231. This work was supported also by Polish national grant from the Ministry of Science and High Education (Grant No. N202-052-32/1189 and N202 142 32/3888) and by German Research Council (DFG project PI 819/1-1). The authors would like to thank D. Hommel (University of Bremen) and D. Lindle (University of Nevada, Las Vegas) for helpful discussions.

References

[1] V.Yu. Davydov, A.A. Klochikhin, V.V. Emtsev, D.A. Kurdyukov, S.V. Ivanov, V.A. Vekshin, F. Bechstedt, J. Furthmüller, J. Aderhold, J. Graul, A.V. Mudryi, H. Harima, A. Hashimoto, A. Yamamoto, E.E. Haller, Phys. Status Solidi B 234 (2002) 787–795.
[2] V. Kachkanov, K.P. O'Donnell, S. Pereira, R.W. Martin, Philos. Mag. 87 (2007) 1999–2017.
[3] S. Figge, C. Tessarek, T. Aschenbrenner, D. Hommel, Phys. Status Solidi B 248 (2011) 1765–1776.
[4] J.J. Rehr, R.C. Albers, Rev. Mod. Phys. 72 (2000) 621–654.
[5] I.N. Demchenko, J.D. Denlinger, M. Chernyshova, K.M. Yu, D.T. Speaks, P. Olalde-Velasco, O. Hemmers, W. Walukiewicz, A. Derkachova, K. Lawniczak-Jablonska, Phys. Rev. B 82 (2010) 075107–075111.
[6] W. Paszkowicz, S. Podsiadlo, R. Minikayev, J. Alloys Compd. 382 (2004) 100–106.
[7] W. Paszkowicz, R. Cerny, S. Krukowski, Powder Diffr. 18 (2003) 14–121.
[8] K. Lawniczak-Jablonska, T. Suski, I. Gorczyca, N.E. Christensen, K.E. Attenkofer, R.C.C. Perera, E.M. Gullikson, J.H. Underwood, D.L. Ederer, Z. Liliental-Weber, Phys. Rev. B 61 (2000) 16623–16632.
[9] C. Lamberti, Surf. Sci. Rep. 53 (2004) 1–197 (among others).
[10] Y. Nanishi, Y. Saito, T. Yamaguchi, Jpn. J. Appl. Phys. 42 (2003) 2549–2559.
[11] Advanced Light Source, soft X-ray fluorescence (SXF) spectrometer, Beamline 8.0.1, 2003, http://www-als.lbl.gov/als/als_users_bl/8.0.1-SXF.pdf.
[12] K.C. Prince, M. Vondráček, J. Karvonen, M. Coreno, R. Camilloni, L. Avaldi, M. de Simone, J. Electr. Spectr. 101–103 (1999) 141–147.
[13] http://www.esrf.eu/UsersAndScience/Experiments/CRG/BM30B/Mendeleev/49-In.html.

[14] D. Doppalapudi, S.N. Basu, K.F. Ludwig, T.D. Moustakas, J. Appl. Phys. 84 (1998) 1389–1395.
[15] A.L. Ankudinov, B. Ravel, J.J. Rehr, S.D. Conradson, Phys. Rev. B 58 (1998) 7565–7576.
[16] Y. Joly, Phys. Rev. B 63 (2001) 125120–125210.
[17] A. Kuzmin, J. Purans, M. Benfatto, C.R. Natoli, Phys. Rev. B 47 (1993) 2480–2486.
[18] T.K. Maurya, S. Kumar, S. Auluck, Optic Commun. 283 (2010) 4655–4661.
[19] T. Mizoguchi, I. Tanaka, S. Yoshioka, M. Kunisu, T. Yamamoto, W.Y. Ching, Phys. Rev. B 70 (2004) 045103–45110.
[20] A.V. Soldatov, A.N. Kravtsova, Condens. Matter. Spectr. 101 (2006) 245–247.
[21] I. Mahboob, T.D. Veal, L.F.J. Piper, C.F. McConville, W.J. Hai Lu, J. Schaff, F. Furthmüller, Bechstedt, Phys. Rev. B 69 (2004) (201307(R)-4).
[22] L.F.J. Piper, L. Colakerol, T. Learmonth, P.-A. Glans, K.E. Smith, F. Fuchs, J. Furthmüller, F. Bechstedt, T.-C. Chen, T.D. Moustakas, J.-H. Guo, Phys. Rev. B 76 (2007) 245204–245205.
[23] S. Eisebitt, W. Eberhardt, J. Electr. Spectr. 110-111 (2000) 335–358.
[24] S. Eisebitt, J. Luning, J.-E. Rubensson, W. Eberhardt, Phys. Status Solidi B 215 (1999) 803–808.
[25] J. Wu, W. Walukiewicz, K.M. Yu, J.W. Ager III, E.E. Haller, H. Lu, W.J. Schaff, Appl. Phys. Lett. 80 (2002) 4741–4743.
[26] F. Bechstedt, J. Furthmüller, M. Ferhat, L.K. Teles, L.M.R. Scolfaro, J.R. Leite, V.Yu. Davydov, O. Ambacher, R. Goldhahn, Phys. Status Solidi A 195 (2003) 628–633.